Tribological behaviour of microalloyed rail steels and conventional C-Mn in pure sliding condition

Journal:	*Part F: Journal of Rail and Rapid Transit*
Manuscript ID	JRRT-17-0128.R1
Manuscript Type:	Article
Date Submitted by the Author:	29-Dec-2017
Complete List of Authors:	Viesca, J; University of Oviedo, González-Cachón, Sergio; Universidad de Oviedo, Department of Construction and Manufacturing Engineering García, Alberto ; Universidad de Oviedo, Department of Construction and Manufacturing Engineering González, Rubén; Universidad de Oviedo, Department of Marine Science and Technology Hernandez Battez, Antolin; University of Oviedo
Keywords:	wear, pin-on-disc, microalloyed steel, rail steels, fine pearlitic microstructure
Abstract:	This paper compares the tribological behaviour of microalloyed rail steel with conventional C-Mn rail steel under different test conditions (load, temperature and humidity). Pin-on-disc tribological tests were performed inside a climate chamber under different loads (20, 30 and 40 N), relative humidity (15, 55 and 70% RH) and temperatures (20 ºC and 40 ºC). After friction and wear tests, worn surfaces were analysed using both confocal and scanning electron microscopy. The results obtained show that the use of microalloyed steel in railway applications under severe conditions (high loads and humidity) could lead to an increased service life for the rail and extend the time between maintenance operations.

Tribological behaviour of microalloyed rail steels and conventional C-Mn in pure sliding condition

J. L. Viesca[a,b,*], S. González-Cachón[a], A. García[a],
R. González[b,c], A. Hernández Battez[a,b]

[a]Department of Construction and Manufacturing Engineering, University of Oviedo, Asturias, Spain
[b]Faculty of Science and Technology, Bournemouth University, UK
[c]Department of Marine Science and Technology, University of Oviedo, Asturias, Spain
[(*)]*Email:* viescajose@uniovi.es / Orcid ID: 0000-0002-9838-8634

Abstract

This paper compares the tribological behaviour of microalloyed rail steel with conventional C-Mn rail steel under different test conditions (load, temperature and humidity). Pin-on-disc tribological tests were performed inside a climate chamber under different loads (20, 30 and 40 N), relative humidity (15, 55 and 70% RH) and temperatures (20 ºC and 40 ºC). After friction and wear tests, worn surfaces were analysed using both confocal and scanning electron microscopy. The results obtained show that the use of microalloyed steel in railway applications under severe conditions (high loads and humidity) could lead to an increased service life for the rail and extend the time between maintenance operations.

Keywords: *wear; pin-on-disc; microalloyed steel; rail steels; fine pearlitic microstructure*

1. Introduction

High-capacity railway lines have grown in number very rapidly in recent years and even more pronounced growth is anticipated in the future. High-speed lines are currently present in more than fifteen countries around the world; although the network is expanding rapidly and is expected to reach 25,000 kilometres of new lines by 2025 (included Saudi Arabia where the first high-speed line that will cross a desert is being built). The development of rails that can be used for new railway infrastructures in extreme environments (high temperature and humidity) should be a priority for the railway industry.

Current rail steels satisfy the needs of the normal loads in service today. However, increasing heavy-haul traffic causes very high levels of wear and deformation on the rail head, which can cause breakage and a significant reduction in the working life of the rail, requiring more frequent replacement.

The railway companies spend billions of dollars a year in maintenance (grinding) and replacement of rails, which has led to the development of new rails with improved mechanical properties (hardness, yield strength and tensile strength) [1], such as the microalloyed steel rails.

The optimum microstructural choice for rail steels is a very fine pearlitic microstructure (reduced interlaminar distance), which improves mechanical properties [2]. For this reason, production of new microalloyed steels has become very popular. This pearlitic microstructure is achieved by adding alloying elements such as niobium, chromium and vanadium. However, the rails produced from these steels have a risk of containing fragile structures such as bainitic and martensitic phases. Little research on microalloyed rail steel has been published to date. Ordoñez et al. [3] studied microstructural factors of premium rail steels that have a direct relation to rail performance. In this case, the appearance of pro-eutectoid cementite at the prior austenite grain boundaries contributed to the development of rolling contact fatigue (RCF) and secondary cracks in the railhead. However, the performance of premium rail steels with respect to impact toughness and wear was better than for conventional steels.

In addition, Panda et al. [4] analysed the nature of oxides generated in Cu and Mo microalloyed rail steels after a service period of two years compared to traditional C-Mn rail steels. The results showed a lower corrosion rate in the case of the Cu–Mo rail steels. Panda et al. [5] demonstrated that microalloyed rail steels have a greater resistance to corrosion than the C-Mn rail steel commonly used. Likewise, Moon et al. [6] evaluated mechanical properties and the influence of hydrogen on microalloyed steels in comparison with conventional steels. The study revealed that the degree of hydrogen embrittlement was higher in C-Mn steel compared to the microalloyed steels. On the other hand, it can be expected that microalloyed steels will have better wear behaviour than C-Mn steels because of their greater hardness. But, Ramalho and Aniołek [7-8] showed that wear in rails does not depend solely on their hardness.

It should be noted that acceptance tests and qualifications included in international standards (EN 13674-1:2011 [9] and AREMA [10]) for steel rails do not require wear tests. Different non-standard tests have been employed in order to study the tribological behaviour of the wheel-rail contact. In addition, research works conducted by Jungwon and Garnham [11-12] indicated that twin-disc configuration is the most suitable configuration to study RCF (rolling contact fatigue) damage on rail surfaces. While other alternative studies [13-14] have shown that the pin-on-disc configuration is also an option for studying wear behaviour in wheel-rail contacts. Windarta and Baharom [15] studied the wear rate of the rail and wheel materials in dry sliding contact using the pin-on-disc configuration and the results were in agreement with results obtained from twin disc configuration.

Wang [16] studied wear and frictional behaviour of rails under high axle loads. The experimental results showed that the decisive factor for the replacement of the rail on the curved sections for heavy traffic lines was the side rail wear. Zhong [17] shows that wear is the main damage in rails used for high loads, while RCF is the main damage in rails used for high-speed lines. Windarta et al. [18] analysed the influence of applied load on wear of rail materials using a pin-on-disc machine. The experimental results showed that wear rate increases proportionally with the increasing of applied load and the main wear mechanism is plastic deformation caused by abrasive wear. Rail wear is related primarily to the nature of the wheel-rail pair (materials, hardness, microstructure, surface finish, etc.) and secondly, with the geometry and contact conditions (pressure, speed, presence of third body, etc.). The researcher Bokowski [19] showed that the wear of the rail does not only depend on its hardness, and also that bainitic steel rails do not have better wear performance than pearlitic steel rails, despite having higher hardness.

Meehan et al. [20] shows that the growth rate of corrugation on the rail has a strong correlation with the variation in environment conditions. In addition, Ishida [21] studied the appearance of corrugation in the surface of the rail and the surface layer of oxide generated in a submarine tunnel, which is influenced by the ambient air of the tunnel, which contains sea salt and high humidity. The results showed that the β-Fe_2O_3. H_2O oxide type that was found on the surface of the rail is causing a reduction in the friction coefficient.

Lewis and Olofsson [22] examined the effects of atmospheric variations and the oxide generated in the performance of friction modifiers (FM) using pin-on-disc testing in a climatic chamber. Oxidative wear (wear particles of Fe_2O_3) was found in the interface between the pin (extracted from the wheel) and the disc (extracted from the rail).

Yi Zhu [23] studied the influence of environmental conditions (temperature and humidity) and iron oxides on the friction coefficient of the wheel-rail contact. The results showed that iron oxides generated on the rail surfaces (Hematite (α-Fe_2O_3)) can increase the coefficient of friction because it is hard and less protective. On the other hand, the effects of boundary lubrication by the water molecule film can reduce the friction coefficient. When neither of the two effects is dominant, the friction coefficient is stabilized.

Recently, Lyu [24] studied the influence of environmental conditions and iron oxides on the wear performance of the wheel-rail contact. The results demonstrated that a low value of relative humidity

(40 % RH) causes adhesive wear, which is increasingly severe with decreasing temperature. However, it was seen that at room temperature and high relative humidity (85 % RH) the main wear mechanism is oxidative wear. This research work focused only on conventional steel rails.

The objective of this paper is to study the tribological behaviour of microalloyed steel rail in comparison with a C-Mn steel rail and the influence of high loads and increased humidity and temperature on friction coefficient and wear.

2. Experimental procedure

2.1 Materials

Steel specimens used for the wear tests were obtained from the profiles of the 54E1 and 115RE rails (**Fig. 1**). These rails have been designed according to the European Standard EN 13674-1:2011 and American Standard AREMA, respectively [9, 10]. Discs and pins for use in wear tests were manufactured from microalloyed steel rail (profile 115RE) and R260 grade C-Mn steel rail (profile 54E1).

Chemical composition and hardness of both steels used were measured and the results were similar to the values established by the previously mentioned international standards. For chemical analysis, samples of the head of the rails were removed in the position indicated by the standard EN 13674-1:2011 and measured using an atomic emission spectrometer by sparking SPECTRO (spectroLAB). The percentage of niobium was measured from steel particles in a plasma mass spectrometer ICP, VARIAN (VISTA-PRO). Pins from both steel rails were used to measure carbon and nitrogen content in specific analysers LECO CS225 and TCH600. Nominal chemical composition of the studied steels is shown in **Table 1**.

Table 1. Measured chemical composition of tested steels.

		Element (wt %)											
Sample	**Rail profile**	**C**	**Mn**	**Si**	**P**	**S**	**N**	**Cu**	**Ni**	**Cr**	**Mo**	**Nb**	**V**
R260	54E1	0.70	1.10	0.26	0.014	0.014	0.005	0.017	0.025	-	-	-	-
Microalloyed	115RE	0.79	1.14	0.43	0.017	0.013	-	-	0.022	0.25	0.003	0.014	0.060

The R260 grade steel is alloyed with manganese, copper and nickel, whereas microalloyed steel includes manganese, molybdenum, chromium, niobium and vanadium. The two steels have different contents of carbon and silicon, but the contents of sulphur, phosphorus and manganese are similar.

The microalloyed steel is much more hardenable than steel R260 because it has a higher percentage of alloy elements (higher content in C and Si). TTT curves of the microalloyed steel are those furthest away from the origin than those of R260 steel because of the microalloys elements dissolved in the austenite delays the formation of bainite and pearlite. It would still be concluded that the hardenability of the steel increases with the addition of the alloy elements, such as silicon and manganese.

The ideal critical diameter (ID) is the hardenability indicator of steel, where the silicon has its importance in its value.

$$\boldsymbol{ID\ (mm) = ID(C) * fm\ (Mn) * fm\ (Si) * fm\ (Cu) * fm\ (Ni) * fm\ (Cr) * fm\ (Mo)}\ \textbf{(1)}$$

$$\boldsymbol{fm\ (Si) = 1 + 0.7 * \%\ Si}\ \textbf{(2)}$$

A higher percentage of microalloys, such as silicon, provide a high-grade alloy steel rail, therefore the residual stress increase in head of the rail [25].

The Brinell hardness measurements were taken on a sample of the head of each rail and were performed according to EN ISO 6506-1 using a Hoytom 1003A durometer. **Table 2** shows the hardness measured, and the rolling surface hardness obtained from the quality certificates supplied by the manufacturer.

Table 2. Measured hardness of tested steels.

Sample	Rail profile	RS Hardness (HB)[a]	Hardness (HB)[b]
R260	54E1	287	249
Microalloyed	115RE	334	292

[a] RS= Rolling surface [b] Hardness of a sample of the head of the rails

Tensile Test measurements were taken on a cylindrical sample of the head of each rail and were performed per UNE-EN 10002-1 using a Universal electromechanical testing machine (Instron) with a load capacity of 100 kN, **Table 3**.

Table 3. Mechanical properties of tested steels.

Sample	Rail profile	Ơy[a] MPa	R[b] MPa	A_5[c] %
R260	54E1	528	951	13
Microalloyed	115RE	677	1150	10

[a] Ơy = Yield Strength [b] R = Breaking Strength [c] A_5 = Elongation

For microstructural characterization, material samples were also extracted from the railhead. These samples were polished and etched with 2% Nital in order to study the inclusions by using confocal microscopy (Leica TCS SP2-AOBS) and electron scanning microscopy (JEOL 5600).

Inclusions were determined in accordance with standard DIN 50602 [26]. The polished surfaces of the samples were observed in an optical microscope at 100 magnifications. Template Nº1 includes four columns with the most common forms of observed inclusions, designated by the number 1, 3, 6, and 8. In turn, each column is formed by templates numbered templates from 0 to 8. The K method of this standard was followed to obtain the level of purity (content of non-metallic inclusions), where the percentage of non-metallic inclusion is determined.

2.2 Wear tests

The wear tests were performed on a fully computerized UMT-3 tribometer using a pin-on-disc configuration, the tribological pairs tested were formed by pins of R260 and microalloyed steels (representing the rail) and discs of R260 steel (representing the wheel). Selection of the R260 steel grade as wheel material is due to its mechanical properties similar to the conventional material used in wheel manufacture [13]. The experiments were conducted using a testing machine designed according to ASTM G99 standards [27].

The wear tests were performed on a tribometer CETR UMT-3 completely computerized with a pin-on-disc configuration. This test method consists in a pin that slides against a rotating disc. The load is applied vertically downwards to a motor-driven adjustable weep carriage, which uses a force/load sensor and a spring to maintain a constant load. During the wear test, the normal forces are applied. Both pin and disc sample are polished using 120, 220 and 500 grit abrasive paper.

The parameters that we can vary to carry out such tests with this tribometer are: load, temperature, velocity, relative humidity and sliding distance (time, cycles). During the tests the friction coefficient are measured in real time. Each test was repeated three times and the results were averaged.

The friction coefficient is measured continuously using a transducer located in the tribometer and sends signals to the computer, which are interpreted by the corresponding software provided by the manufacturer. The wear of pins specimens are determined as the average weight losses, which were measured before and after each test, using a scale with 0.5 mg resolution. The pins before any

weighed are cleaned with heptane in an ultrasonic bath for 10 minutes, then dried with hot air to remove any residual solvent.

Tribological tests for different atmospheric conditions (humidity and temperature) were carried out in a climatic chamber with the control of temperature and humidity. SEM JEOL 5600 with EDX scanning electron microscope was used to examine and evaluate the wear mechanism on pins after the wear tests.

Discs of 69.85 mm diameter and 6.60 mm thickness were taken from the foot of the 54E1 rail profile (R260 grade). The pins of 6.3 mm diameter and 18.8 mm length were taken from the head of the rail 115RE (microalloyed) and 54E1 (R260 grade) profiles. Both specimens were finished to a surface roughness Rq = 0.5μm.

In order to study the influence of high loads on the wear behaviour of microalloyed and C-Mn rail steels, pin-on-discs tests were conducted at room conditions (20 ºC 55 % RH), under three normal loads 20, 30 and 40 N, 200 rpm (corresponding to 0.52 m/s) and 60-min duration (sliding distance = 1.88 km). Each test was replicated at least three times. These test conditions in agreement with previous research work in the study of the wear behaviour of steel rails [13, 14, 15, 18, 28, and 29].

Additional tests for the study of the influence of atmospheric variables on the tribological behaviour of the rail steel were performed in a climatic chamber to control temperature and relative air humidity. Pin-on-disc testing was carried out under a normal load of 20 N, at 200 rpm (0.35 m/s), with 60-min duration (sliding distance = 1.28 km) and for different levels of relative humidity (15 and 70 % RH) and temperature (20 ºC and 40 ºC). Each test was also replicated at least three times. The higher relative humidity value studied (70 %) corresponds to the typical conditions in underground tunnels [22], where high wear rate has been found mainly due to high relative humidity. On the other hand, temperatures of 40 ºC with 15 % RH are conditions typical of an arid climate [30].

Before and after wear tests, the specimens were cleaned with heptane in an ultrasonic bath for five minutes and dried with hot air. Wear (mass and volume) of the pins was measured by a precision balance (with a precision up to 0.5 mg). Wear surfaces of the pins were also analysed with optical microscopy (Nikon EPIPHOT 200) and scanning electron microscopy (MEB JEOL-6610LV) in order to evaluate the wear mechanism.

3. Results and discussion

3.1 Microstructural analysis

Fig. 2 shows non-metallic inclusions of MnS dispersed in the pearlitic matrix of both steel samples. The inclusions percentage was similar in both cases **according to the method described above**; however their morphology and distribution were different depending on whether samples were extracted in longitudinal or transversal direction. The inclusions in transversal direction, **Fig. 2a**, are smaller in size and have a globular morphology; while in longitudinal direction they are narrower and longer, **Fig. 2b and 2c**.

Fig. 2c shows an alignment of inclusions in the microalloyed steels, in addition to the staggered orientation of the inclusions in the rolling direction. **The alignment of inclusions is related with the rolling direction, and this effect is more relevant in microalloyed steel due to the higher degree of deformation during the rolling process. Microalloyed steel samples were extracted from 115 RE rail profiles, while R260 steel samples were obtained from 54E1 rail profile.**

Therefore, non-metallic inclusions are more deformed, more crushed (thinner and longer particles) and preferably oriented in the rolling direction in microalloyed steel. Fig. 3 shows the differences between the two rail profiles used.

This can influence fatigue crack growth in the longitudinal direction [31]. In summary, the profile rolling process of microalloyed steel rail will affect the distribution and the morphology of the metal inclusions, which occur mainly in the rolling direction, increasing the rate of fatigue crack growth in the longitudinal plane of microalloyed steel rail and significantly reducing its fatigue behaviour [32].

Fig. 4 shows that both steels have a fully pearlitic microstructure without presence of ferrite in the grain boundary and no fragile microstructures such as bainite, martensite or cementite. Both steels studied have the desired microstructure (pearlite), which improves the mechanical properties for use in severe track conditions. For both steels a morphological analysis was performed, measuring the interlaminar spacing using the intersection procedure described by Underwood [33]. The interlaminar spacing of the microalloyed steel (**Fig. 5a**) is less than that of the R260 steel (**Fig. 5b**). Microalloyed steel perlite is thinner than that of the C-Mn steel and that is why the former has improved mechanical properties (higher tensile strength, yield strength and hardness), **Tables 2-3**.

The reason why this occurs is that the lower the thickness of the ferrite layer, the higher is the probability of the dislocations being immobilized and piling on top of each other if an obstacle is encountered during movement, which means that it is necessary to apply a lot stress to get them moving again. As a result, mechanical resistance properties increase.

Furthermore, the microalloyed steel rail has a higher hardness than the C-Mn steel rail (**Table 2**) due to its higher content of carbon and alloying elements (especially manganese and vanadium), which provide a superior hardening effect. The presence of vanadium and niobium act as carburigen elements which delay austenitic transformation and allow precipitation hardening, thus obtaining a fine perlite (**Fig. 5**) with improved mechanical properties. The hardness, the yield strength and the breaking strength increase with a decrease in the interlaminar spacing, while elongation increases in value with an increase in the interlaminar spacing.

3.2 Tribological tests for high loads

Fig. 6 shows mean values and deviation of pin wear (mass loss) after tribological tests. It can be seen that R260 steel pins exhibited higher wear than the microalloyed steel pins for the three applied loads (20, 30 and 40 N). Both steels show the same increasing trend of wear with the increase in applied load.

Fig. 7 and Fig. 8 show the wear surfaces of the steel pins after tribological tests. The appearance of adhesion joints was observed on the wear surfaces of both tested steels. **The adhesion joints are marked with a red circle, which had already been observed in the research carried out by Viáfara [29].** The increase in load leads to an increase in the severity of wear (more plastic deformation and formation of cracks on the surface). Adhesive wear was the wear mechanism observed in both cases, being more severe in the R260 steel. The results obtained demonstrate that the microalloyed steel has higher wear resistance than the R260 steel. **Fig. 9 and Fig. 10 show the worn surfaces of the pins of the R260 and microalloyed steels at 20 N captured with optical microscope.**

The Archard wear model [34] describes the loss of material. According to this model the volume of wear (m^3) is proportional to the wear coefficient k, the normal force N (N) and the sliding distance S (m), and inversely proportional to the hardness H (N/m^2) of the softer material in the contact.

$$\boldsymbol{V = (k * N * S)/H} \quad \textbf{(3)}$$

Fig. 11 shows the change in adhesive wear coefficient (k) on increasing the applied load for each of the studied steels. A high value of wear coefficient (k) indicates lower wear resistance; so the microalloyed steel exhibits greater wear resistance than the R260 steel. A conclusion can be derived from this graph: the wear coefficient (k) for the microalloyed steel remains stable at increasing applied load.

On the other hand, the wear coefficient of the R260 steel decreases with the increase in applied load, **the change in K wear coefficient probably indicates changes in the wear mechanisms, as it has been reported by Lewis et al. [35]. In R260 samples, pin and disc are made from the same material, and as a result, the adhesion wear mechanism is more suitable. Fig. 12 and Fig. 13 show these changes in the main wear mechanism for steel R260.**

Fig. 14 and Fig. 15 show the friction coefficient variation with time and the applied load. Although the wear behaviour of the two steels was quite different under the testing conditions employed, no significant differences were observed in friction coefficient. **The slight differences between low and high load COF evolution cannot be considered due to the natural variability of the test.**

The evolution of friction coefficient with time was similar for both steels studied; the same conclusion was reached in the study conducted by Viáfara [29].

For both steels used in this study, the friction coefficient increases rapidly to values between 0.5-0.7 and at the end of tests the average coefficient of friction reached a value of 0.6. This result was also observed by Dayot [36]. The average friction coefficient of 0.6 obtained during these tests was slightly higher than the 0.45 value obtained in a previous study under similar conditions [37].

3.3 Tribological tests under different atmospheric conditions (temperature and humidity)

The mass loss of R260 and microalloyed steel pins for the two relative humidities studied (15% RH and 70% RH) and at room temperature is shown in **Fig. 16a**. The results show that the two steels tested with high relative humidity have greater mass loss than the samples tested at lower relative humidity. The two studied steels are equally sensitive to the increase in the humidity.

The mass loss of R260 and microalloyed steel pins for the two temperatures studied (40 ºC and 20 ºC) and for 15 % RH is shown in **Fig. 16b**. The results show that the two steels tested at a temperature of 40 ºC have the same mass loss as at 20ºC, and respond in the same way to the increase in the temperature.

In order to explore the different wear mechanisms for diverse environments, the surface topography marks of wear on the pins has been studied with the Scanning Electron Microscope (SEM). **Fig. 17 and**

Fig. 18 show SEM images of the wear surface from the microalloyed pins after tribological tests at 70 % RH and room temperature (20 ºC).

As can be seen in **Fig. 17**, the growing stresses lead to the formation of microcracks (the starting point of the damage), which with time propagate to the surface, and unite with other cracks, until small quantities of the material are detached, causing the pitting or spalling of the surface. **Fig. 17** clearly shows adhesive wear caused by plastic deformation.

We can see in this figure that the crop marks associated with the propagation of cracks parallel to the direction of sliding. **Fig. 18** shows a photograph of the remains of the disc test piece adhered to the pin material with the formation of adhesion joints (characteristics of adhesive wear).

Fig. 19 and Fig. 20 show the variation in the coefficient of friction with time and humidity applied to the R260 and microalloyed steels. It can be seen that that the evolution of friction coefficient with time increases for the lower humidity studied. The variation in relative humidity had an influence on wear resistance and has also had a marked effect on the friction coefficient, which is greater for the lower relative humidity studied (15 % RH) caused by water condensation. Water condensation could have a significant effect on boundary lubrication on the contact surfaces, which happens when the friction surfaces are separated by a thin film of water condensation. This film of water which is formed at high levels of humidity (70% RH) may maintain the oxides on the surface, and reduce the friction coefficient [23].

Fig. 21 shows the micro-analysis of the wear surface obtained from energy dispersive spectroscopy (EDS) where only the elements present in steel were found. In addition, all the samples studied show oxidation, which is indicated by the presence of a small percentage of oxygen in each of the samples studied (1-3 % O). The research performed by Suzumura [38] who analysed the oxides generated on the surface of the rail by x-ray diffraction, also showed that the amount of rust produced was very small.

Table 4. Semi quantitative elemental analysis from points marked on Fig. 16.

Point	C (%)	O (%)	Fe (%)	Total (%)
1	15.26	2.69	82.05	100
2	13.43	1.89	84.68	100
3	10.67	1.01	88.31	100

4. Conclusions

From the results obtained in this study some conclusions can be drawn:

- Microalloyed steels have greater wear resistance than C-Mn steels, based on their mechanical properties (such as hardness, yield strength and tensile strength). This is associated with smaller interlaminar spacing, because of the concentration of carbon, manganese and chromium in the microalloyed steel, which allows a fine pearlitic microstructure.
- The R260 steel pins exhibited greater wear than the microalloyed steel pins for the three loads applied (20, 30 and 40 N), and both steels show the same trend to increased wear with the increase in the applied load.
- The wear coefficient (k) for the microalloyed steel rail is not sensitive to the increase in applied load. In addition, the wear coefficient of the R260 steel rail decreases with the increase in applied load.
- The microalloyed and R260 steels tested at high relative humidity have greater mass loss than those tested at lower relative humidity and the two steels are equally sensitive to the increase in humidity. However, an increase in temperature has no influence on the wear of microalloyed and R260 steels rail within the 20-40 ºC range.
- The friction coefficient is greater at the lower relative humidity (15 % RH) than for the highest relative humidity (70 % RH) due to water condensation.
- The use of microalloyed steel rather than C-Mn steel in severe track conditions results in longer service life and increases the time between maintenance operations.

Acknowledgments

The authors want to thank to the Foundation for the Promotion in Asturias of Applied Scientific Research and Technology (FICYT) for supporting this work within the framework of the research project 'Lubrication and Surface Technology - LUSUTEC' (GRUPIN14-023).

References

[1] Wang J, Zhou H, Shi Y and Feng B. Mechanical properties and fracture toughness of rail steels and thermite welds at low temperature. International Journal of Minerals, Metallurgy and Materials 2012; 19: 409-420.

[2] Perez-Unzueta AJ and Beynon J. Microstructure and wear resistance of perlitic steel rails. Wear 1993; 162: 173-182.

[3] Ordóñez R, García CI, Ardoa A, Kalay S and Robles FC. Advanced metallurgical alloy design and thermomechanical processing for Steel rails for North American heavy haul use. Wear 2011; 274: 364-373

[4] Panda B, Balasubramaniam R, Vajpei AC, Srikanth S and Bhattachary A. Characterization of rust on microalloyed steel rail exposed to coastal location in India. Engineering, Science and Technology 2009; 44: 275-279.

[5] Panda B, Balasubramaniam R and Moon A. Microstructure and mechanical properties of novel steel rails. Materials Science and Technology 2009; 25: 1375-1382.

[6] Moon AP, Balasubramaniam R and Panda B. Hydrogen embrittlement of microalloyed steel rails. Materials Science and Engineering 2010; 527: 3259–3263.

[7] Ramalho A, Esteves M and Marta P. Friction and wear behavior of rolling–sliding steel contacts. Wear 2013; 302: 1468-1480.

[8] Aniołek K and Herian J. The structure, properties and a resistance to abrasive wear of railway sections of steel with different pearlite morphology. IOP Conf. Series: Materials Science and Engineering 2011; 22: 012012.

[9] EN 13674-1: 2011 Railway applications - Track - Rail - Part 1: Vignole railway rails 46 kg/m and above.

[10] AREMA (The American Railway Engineering and Maintenance-of-Way Association). Manual for railway engineering 2013; Vol. 1 Track: Ch. 4 – Rail.

[11] Jungwon S, Seokjin K and Deonghyeong L. Effects of surface defects on rolling contact fatigue of rail. Procedia Engineering 2011; 10: 1274–1278.

[12] Garnham JE and Davis CL. Very early stage rolling contact fatigue crack growth in pearlitic rail steels. Wear 2011; 27:100-112.

[13] Ozsarac U and Aslanlar S. Wear behavior investigation of wheel/rail interface in water lubrication and dry friction. Industrial Lubrication and Tribology 2008; 60: 101-107.

[14] Shariff SM, Pal TK, Padmanabham G and Joshi SV. Sliding wear behaviour of laser surface modified pearlitic steel rail. Surface Engineering 2010; 26: 199-208.

[15] Windarta and Baharom MB. Experimental prediction of wear rate on rail and wheel materials at dry sliding contact. MATEC Web of Conferences 2014; 13: 3-13.

[16] Wang WJ, Guo HM, Du X, Guon J, Liu QY and Zhu MH. Investigation on the damage mechanism and prevention of heavy-haul railway rail. Engineering Failure Analysis 2013; 35: 206-218.

[17] Zhong W, Hu JJ, Shen P, Wang CY and Lius QY. Experimental investigation between rolling contact fatigue and wear of high-speed and heavy-haul railway and selection of rail material. Wear 2011; 271: 2485-2493.

[18] Windarta MB and Sudin KF. Influence of applied load on wear characterizations of rail material. Journal of Applied Sciences 2011; 11: 1636-1641. [

[19] Bakowski H, Posmyk A, Krawczyk J. Tribological properties of rail steel in straight moderately loaded sections of railway tracks. Archives of Metallurgy and Materials 2011; 56: 813-822.

[20] Meehan PA, Bellette PA and Horwood RJ. Does god play dice with corrugations? Environmental effects on growth. Wear 2014; 314: 254-260.

[21] Ishida M, Aoki F , Sone Y, Ban T and Shirouzu K. Rail corrugations caused by low coefficient of friction in a submarine railway tunnel. Proceedings of the World Tribology Congress III, Washington, D.C. 2005: 931-932.

[22] Lewis S, Lewis R, Olofsson U, Eadie DT, Cotter J and Lu X. Effect of humidity, temperature and railhead contamination on the performance of friction modifiers: Pin-on-disk study. Proceedings of the Institution of Mechanical Engineers, Part F: Journal of Rail and Rapid Transit 2013; 227: 115-127.

[23] Zhu Y, Olofsson U and Chen H. Friction between Wheel and Rail: A Pin-On-Disc Study of Environmental Conditions and Iron Oxides. Tribology Letters 2013; 52: 327-339.

[24] Lyu Y, Zhu Y and Olofsson U. Wear between wheel and rail: A pin-on-disc study of environmental conditions and iron oxides. Wear 2015; 329: 277-285.

[25] González Fueyo JL. Influencia de la microestructura en el comportamiento mecánico de aceros utilizados en la fabricación de carril. Thesis of the University of Oviedo 1997.

[26] DIN 50602. Microscopic examination of special steels using standard diagrams to assess the content of non-metallic inclusions (1985).

[27] ASTM G99 – 17: Standard Test Method for Wear Testing with a Pin-on-Disk Apparatus.

[28] Windarta M, Sudin B and Baharom MB. Prediction of Contact Temperature on Interaction between Rail and Wheel Materials Using Pin-on-Disc Method. Journal of Applied Sciences 2012; 12: 2424-2429.

[29] Viáfara CC, Castro MI, Vélez JM and Toro A. Unlubricated sliding wear of pearlitic and bainitic steels. Wear 2005; 259: 405-411.

[30] United Arabian Emirates climate. Whether online, 24 June 2017.

[31] Qi J, Zhu W, Yang C, Ou T, Chen J and Liu Y. MnS inclusion behaviour in heavy rail steel during heating process. Heat Treatment of Metals 2013; 38: 40-42.

[32] El-Shabasy AB and Lewandowski JJ. Effects of load ratio, R, and test temperature on fatigue crack growth of fully pearlitic eutectoid steel (fatigue crack growth of pearlitic steel). International Journal of Fatigue 2004; 26: 305-309.

[32] Underwood EE. Quantitative Stereology. Addison-Wesley Reading, Massachusetts, 1970.

[34] Archard JF and Hirst W. Wear of metals under unlubricated conditions. Proc. R. Soc. London Part A, 1956; 236: 3–55.

[35] Lewis R and Olofsson U. Mapping rail wear regimes and transitions. Wear 2004; 257: 721–729.

[36] Dayot C, Saulot A, Godeau C and Berthier Y. Tribological behaviour of pearlitic and bainitic steel grades under various sliding conditions. Tribology International 2012; 46: 128-136.

[37] Tyfour WR, Beynon JH, Kapoor A. The steady wear behavior of pearlitic steel rail under dry rolling–sliding contact conditions. Wear 1995; 180: 79–89.

[38] Suzumura J, Yasutomo S, Ishizaki A, Yamashita D, Nakajima Y, Ishida M. In situ X-ray analytical study on the alteration process of iron oxide layers at the railhead surface while under railway traffic. Wear 2011; 271: 47-53.

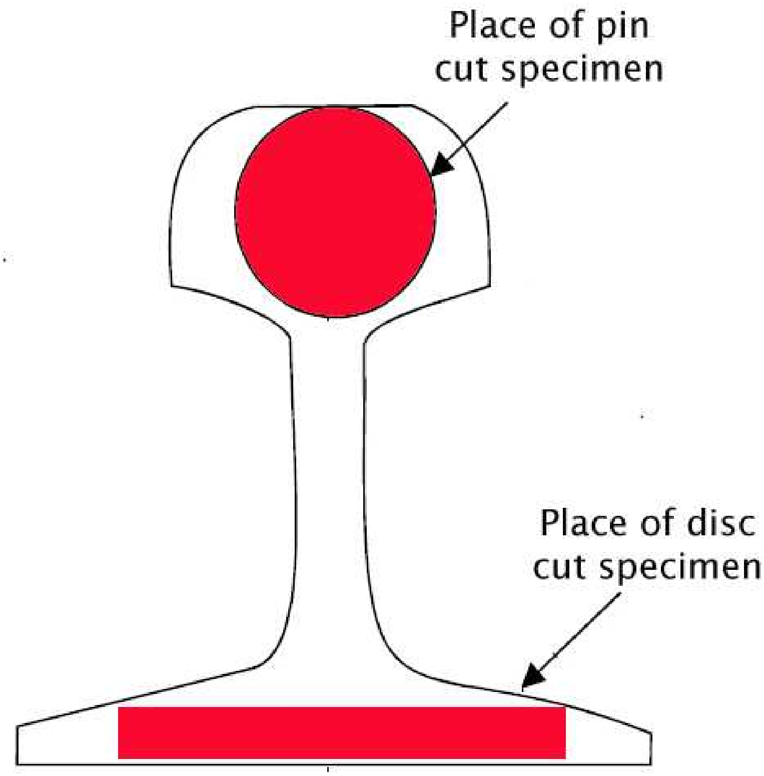

Fig. 1. Extraction zone of the specimens for the wear tests.

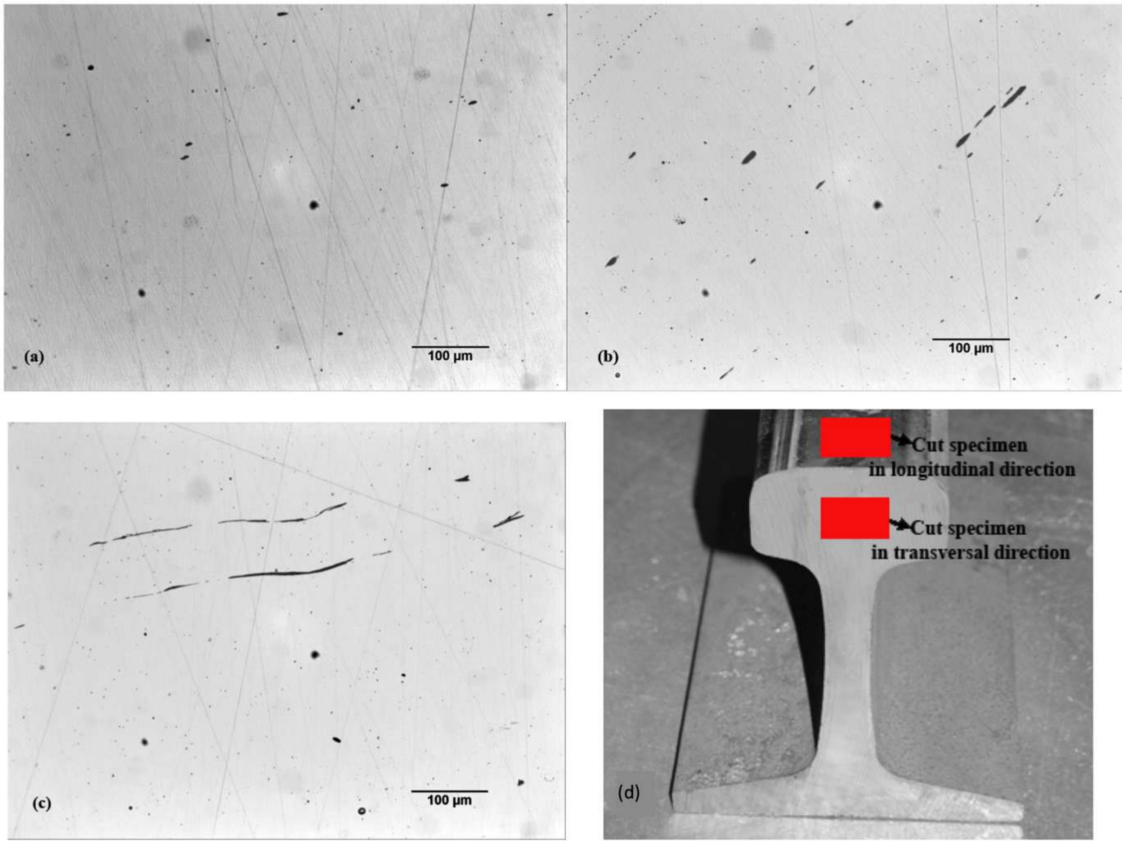

Fig. 2. Inclusions in the rails: (a) R260 steel in the transversal direction, (b) R260 steel in the longitudinal direction, (c) microalloyed steel in the longitudinal direction and (d) cutting directions.

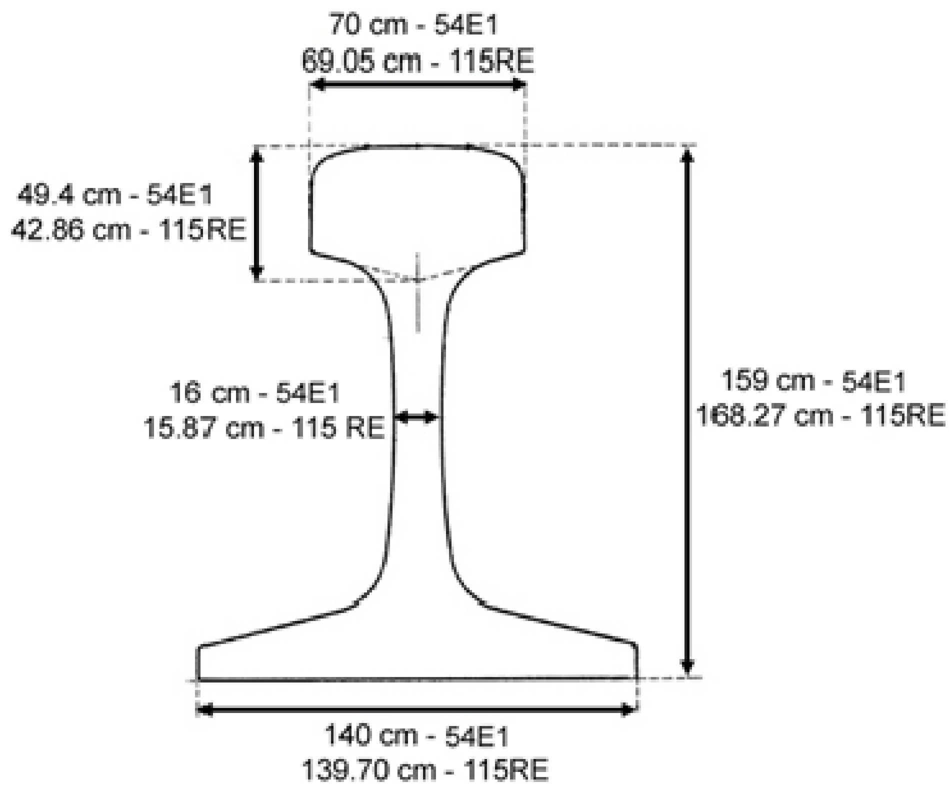

Fig. 3. Profile design according to the standards: EN 13674-1:2012 (54E1) and AREMA (115RE).

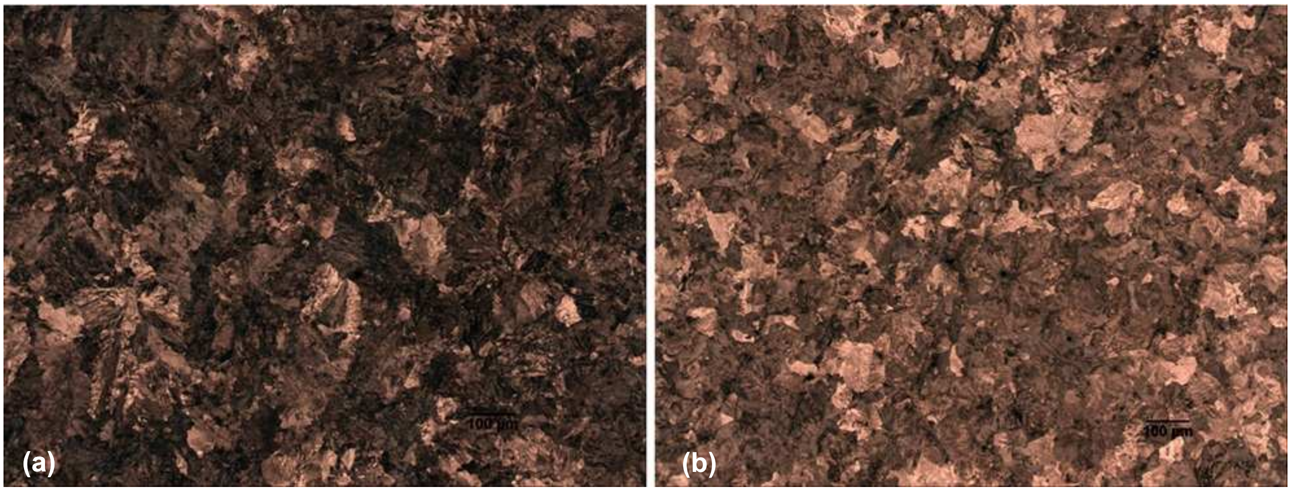

Fig. 4. Pearlitic microstructure: (a) R260 steel (b) microalloyed steel.

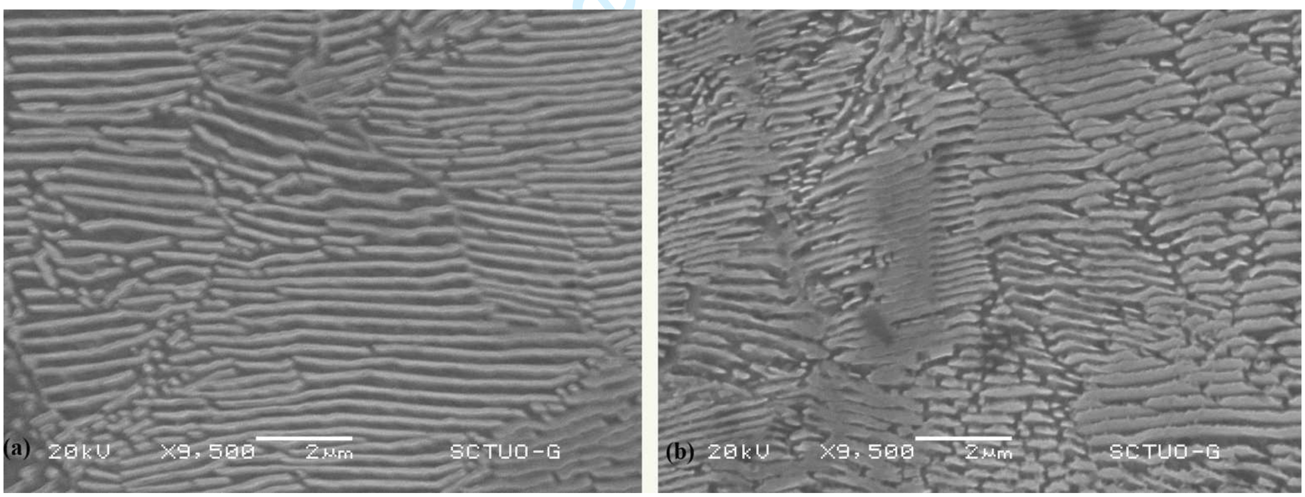

Fig. 5. Morphological analysis. (a) Microstructure R260 steel (9500X) and (b) microstructure microalloyed steel (9500X).

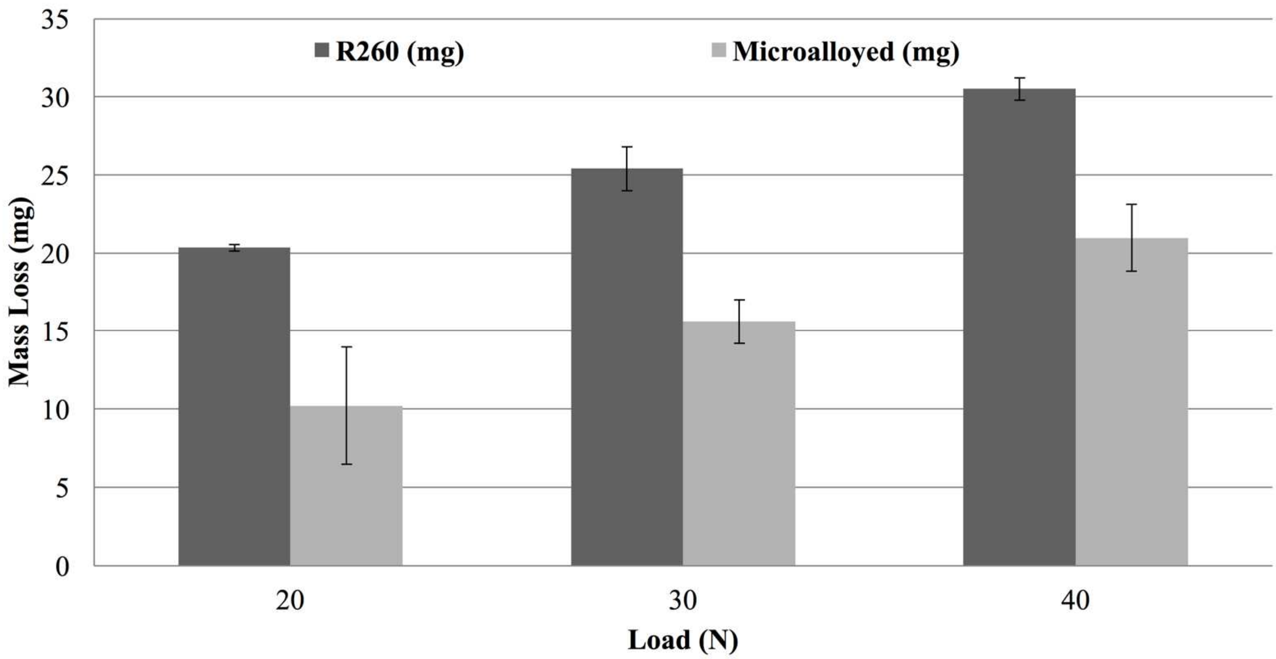

Fig.6. Wear (mass loss) with respect to the applied load.

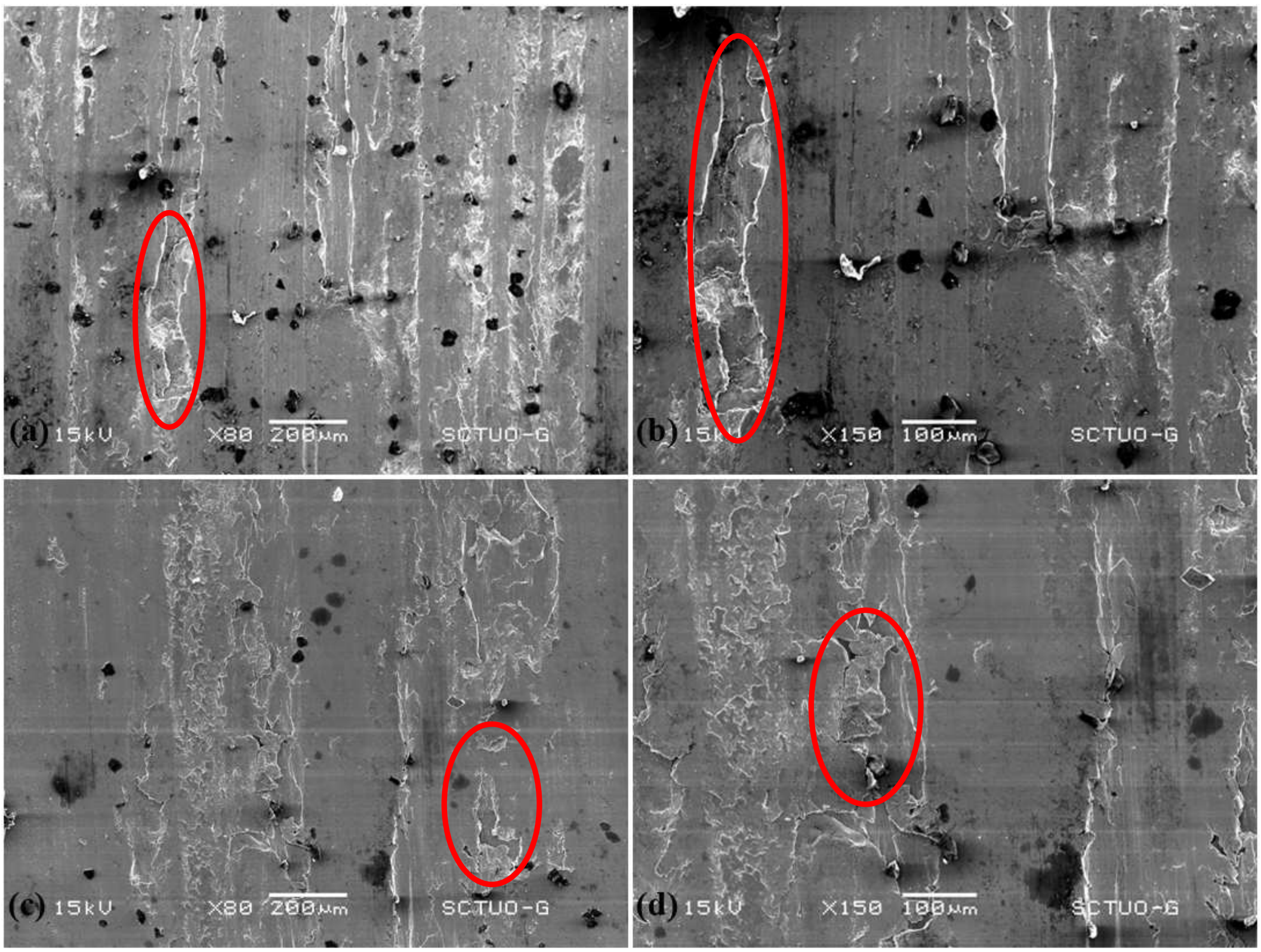

Fig. 7. SEM images of wear surface of the R260 steel pin. (a) 20 N, 80X, (b) 20 N, 150X, (c) 40 N, 80X and (d) 40 N, 150X.

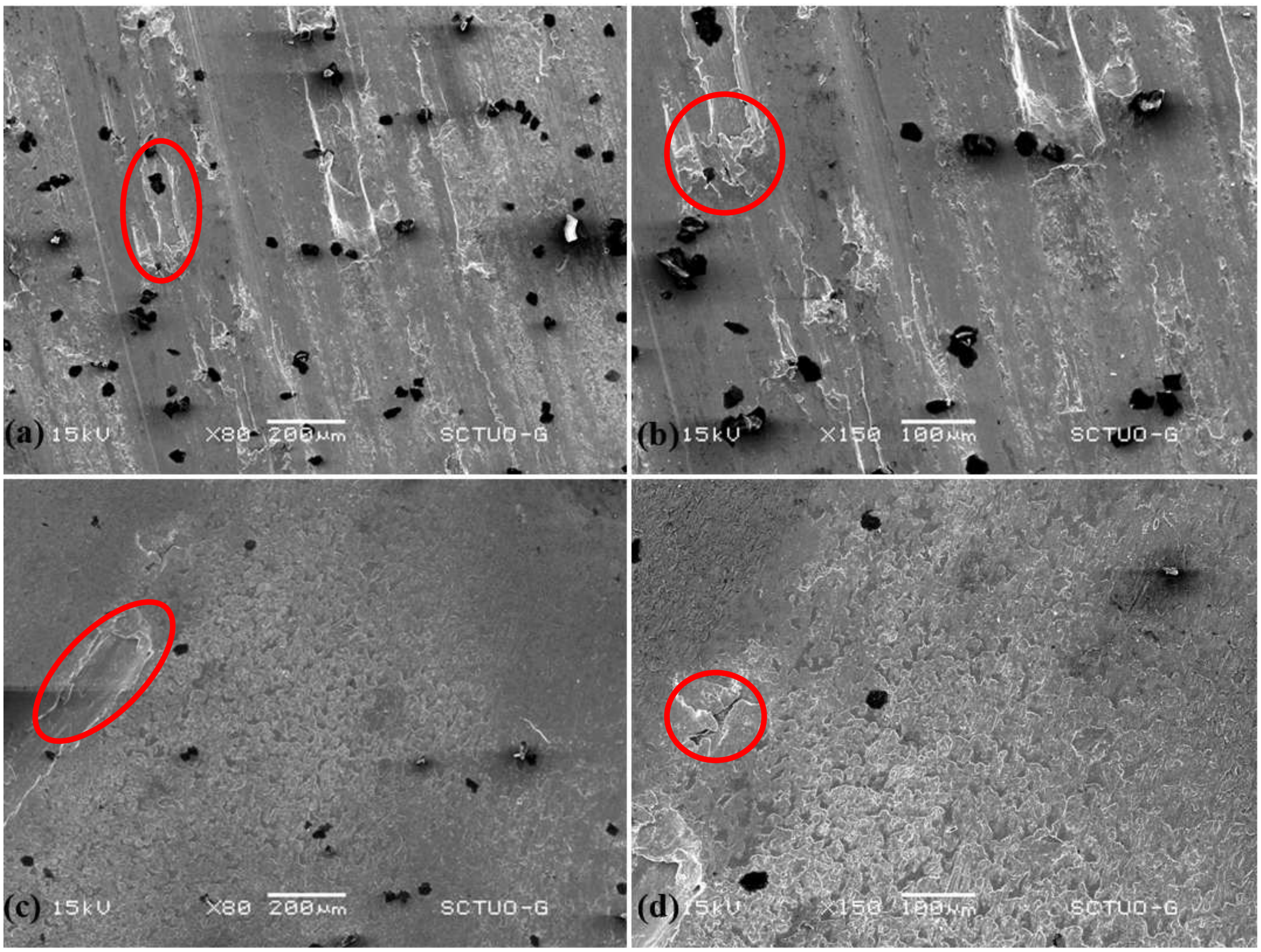

Fig. 8. SEM images of wear surface of the microalloyed steel pin: (a) 20 N, 80X, (b) 20 N, 150X, (c) 40 N, 80X and (d) 40 N, 150X.

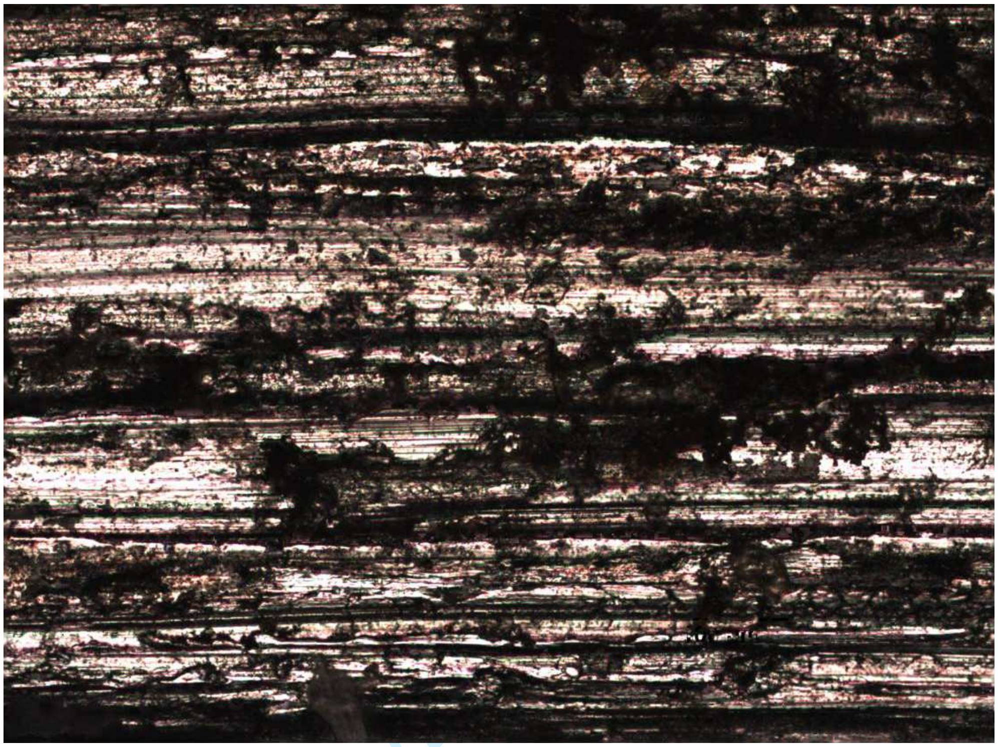

Fig. 9. R260-20 N steel pin worn surface, 200X.

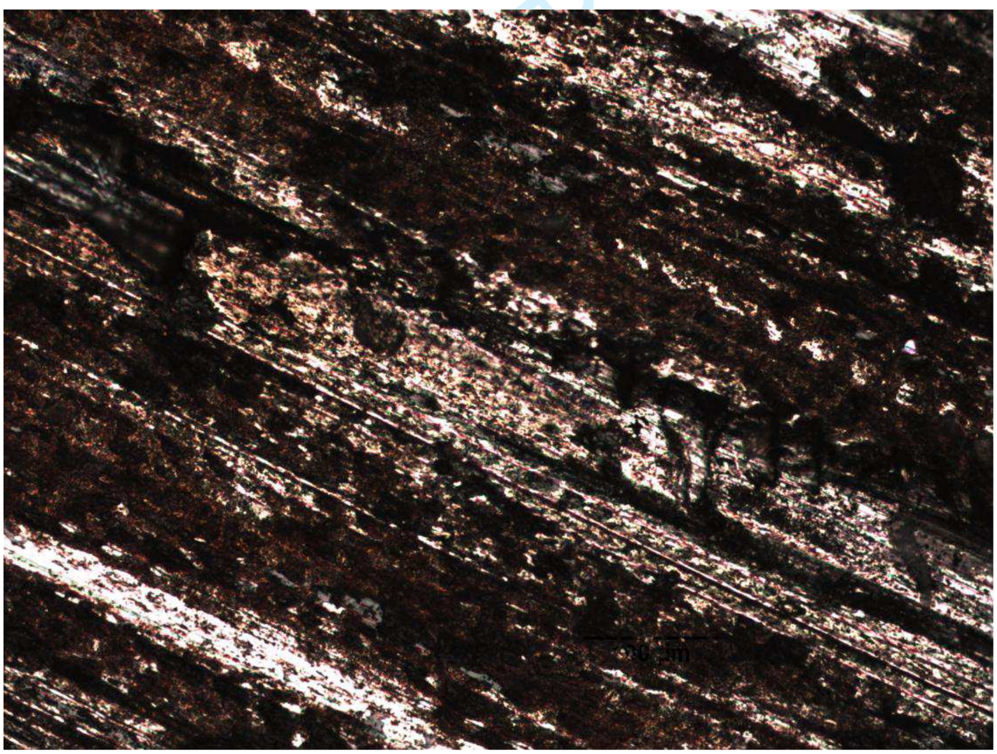

Fig. 10. Microalloyed-20 N steel pin worn surface, 200X.

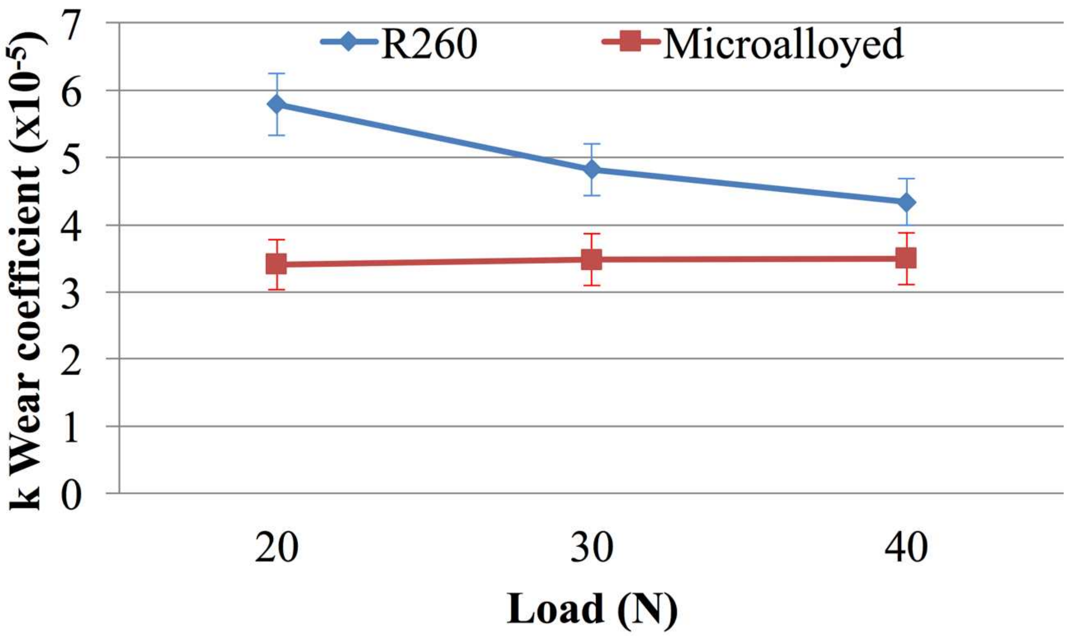

Fig. 11. Wear coefficient (k).

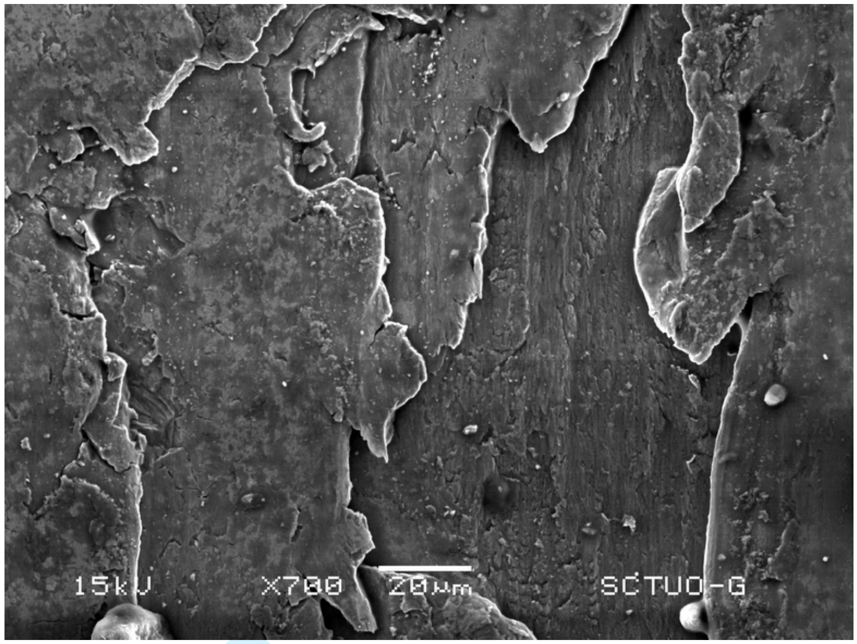

Fig. 12. Adhesive wear mechanism R260-40N steel pin.

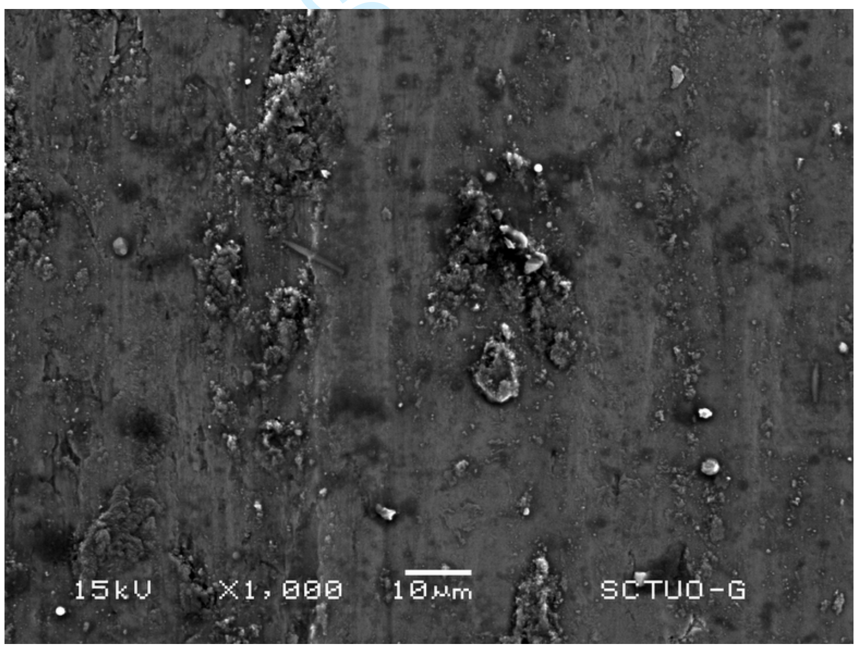

Fig. 13. Abrasive wear mechanism R260-20N steel pin.

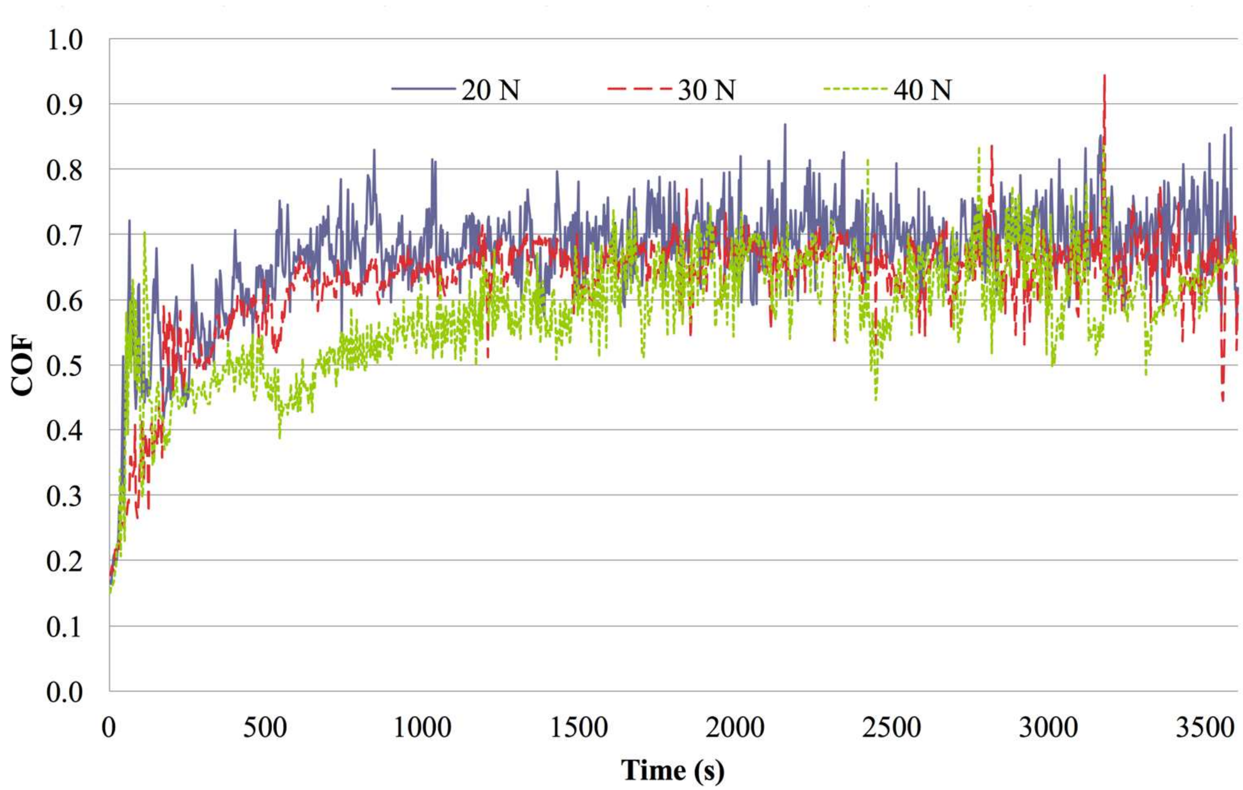

Fig. 14. Variation of friction coefficient with time for the R260 steel.

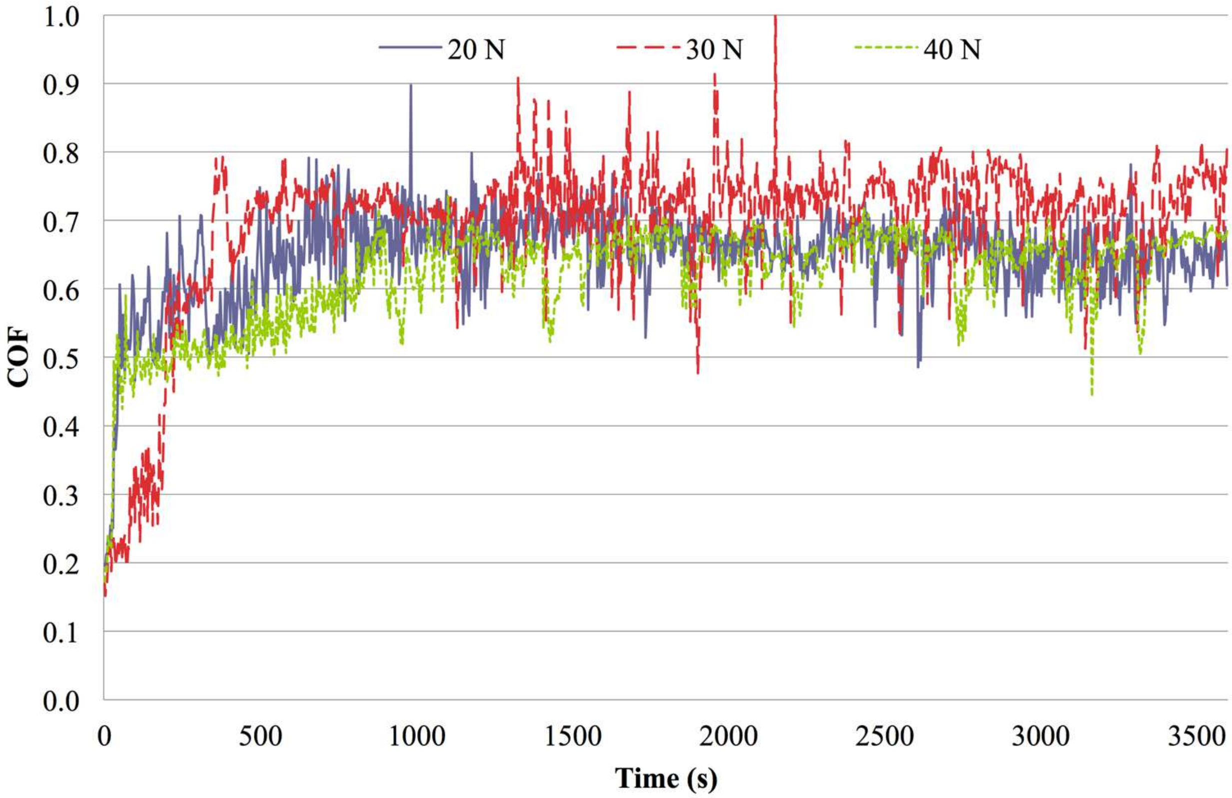

Fig. 15. Variation of friction coefficient with time for the microalloyed steel.

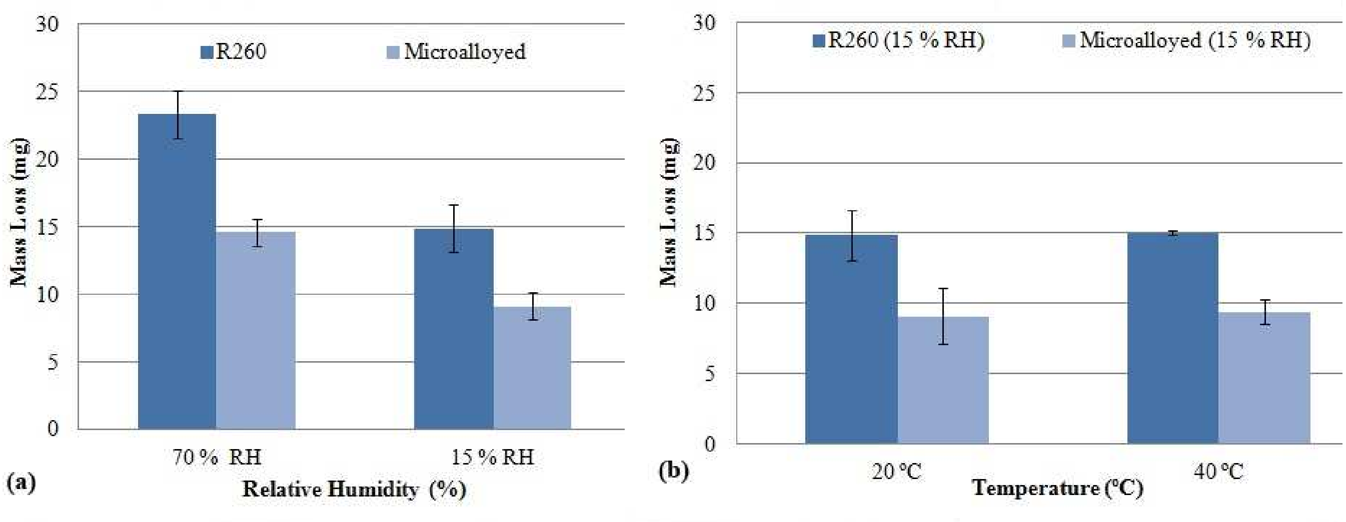

Fig. 16. Comparison of mass loss according to the type of steel studied.

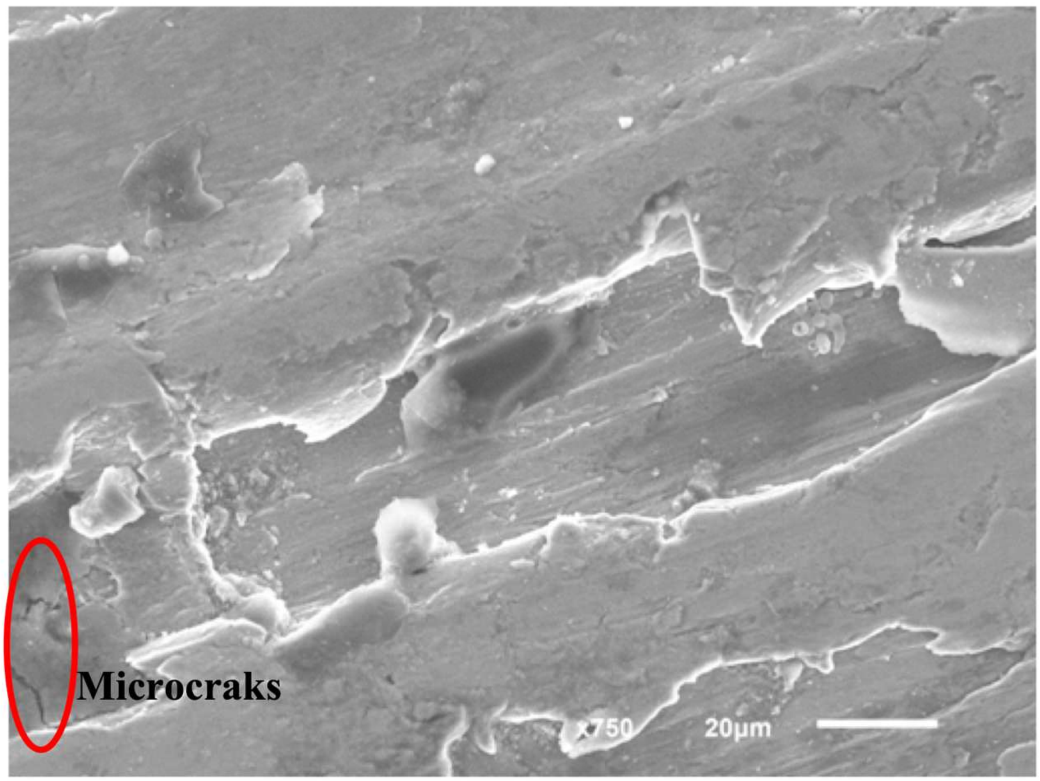

Fig. 17. Wear surface from the microalloyed pins (70 % and 20 ºC).

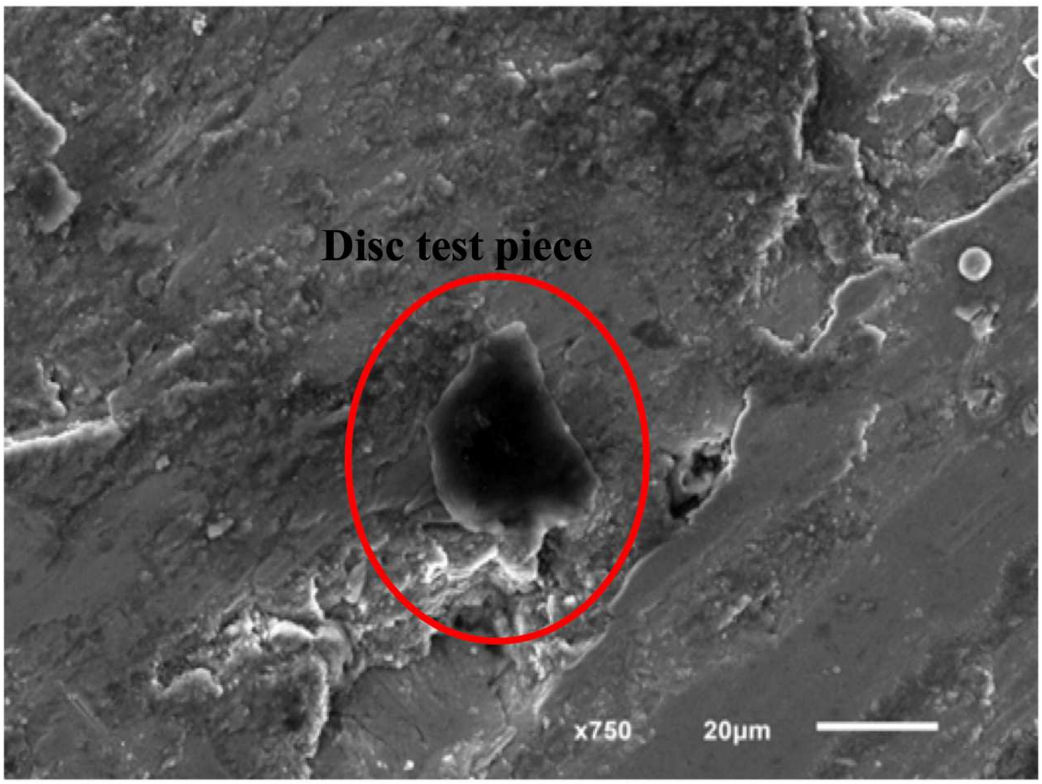

Fig. 18. Adhesion joints and material transferred from the disc.

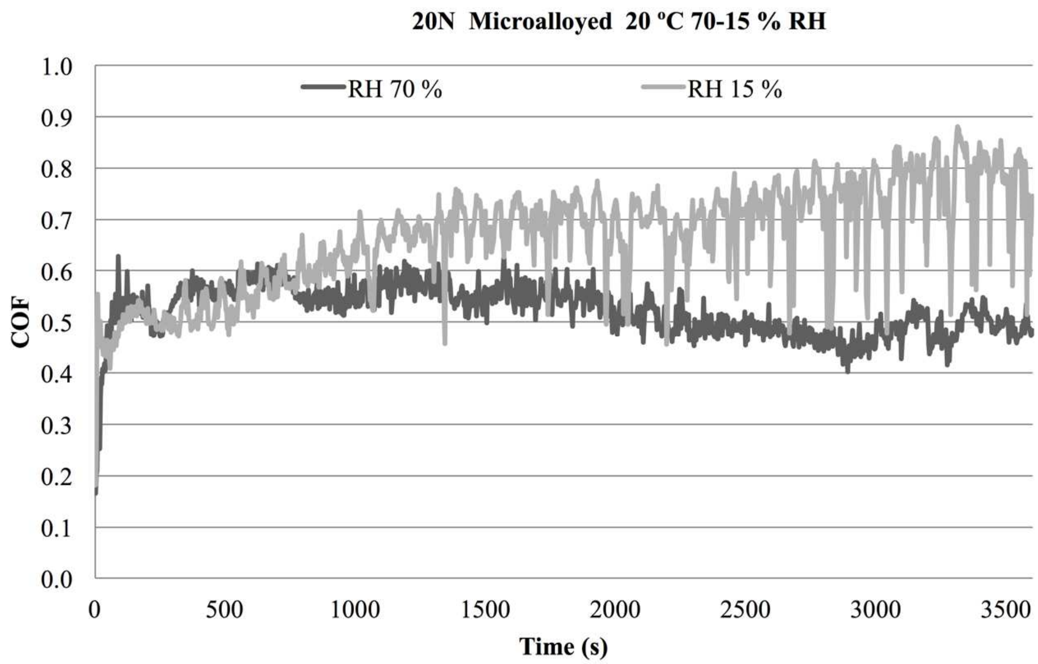

Fig. 19. Variation in friction coefficient with time for the microalloyed steel (20ºC).

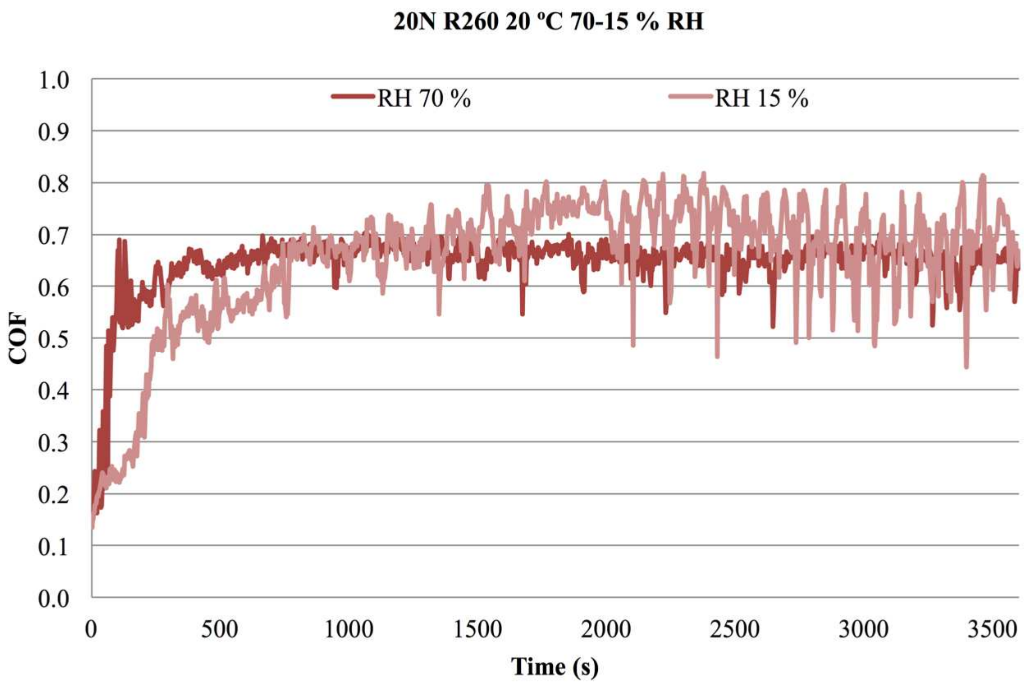

Fig. 20. Variation in friction coefficient with time for the R260 steel (20ºC).

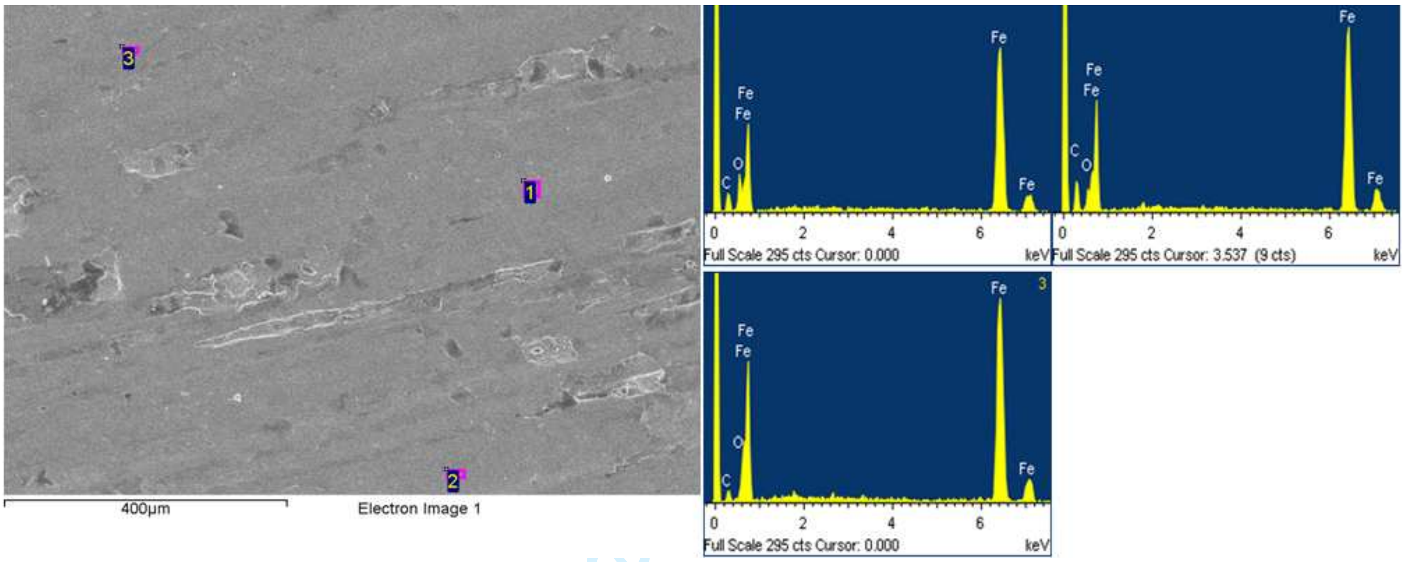

Fig. 21 SEM image and EDS analysis from the wear surface after tests made at 70 % RH and 40 ºC.